論文 / 著書情報
Article / Book Information

Title	Effect of elastic element on self-excited electrostatic actuator
Authors	Hiroyuki Nabae, Koichi Ikeda
Citation	Sensors and Actuators A: Physical, Vol. 279, pp. 725-732
Pub. date	2018, 8
DOI	http://dx.doi.org/https://doi.org/10.1016/j.sna.2018.06.045
Creative Commons	See next page.
Note	This file is author (final) version.

License

Effect of Elastic Element on Self-excited Electrostatic Actuator

Hiroyuki Nabae, Koichi Ikeda

Department of Mechanical Engineering, School of Engineering, Tokyo Institute of Technology, 2-12-1 Ookayama, Megro-ku, Tokyo 152-8550, Japan

Abstract

Self-excited electrostatic actuators, which are also called Franklin bells or Gordon bells, are one of the simplest oscillators among various types of actuators. The actuators oscillate with DC voltage and simple structures mainly composed of only two electrodes and a conductive armature. These features seem suitable for micro mechatronic devices, including micro robots; however, these actuators only have small number of practical applications. The high voltage for actuation, damage by electrical discharge, and mechanical loss with collisions between the armature and electrodes keep the actuators away from practical usages. This research focuses on the mechanical loss with collisions between the armature and electrodes and proposes a method for decreasing this loss by energy recovery with elastic elements. This study first conducts a model-based analysis of the behavior of the proposed system that combines the electrostatic self-excitation and the elastic elements. The results are then compared with the experimental results of a prototype actuator. The simple analysis predicted the increase of the oscillating frequency with the elastic elements, limiting the condition of the self-excitation caused by the energy loss of the damping factor. The results of the experimental verification showed the same tendency as the analytical predictions: increase of the oscillating frequency and existence of a critical value for the oscillation limit. Although comparatively large errors were confirmed between the simulation and the experiment under a lower applied voltage, experimentally obtained frequencies have errors less than 6.4% compared with the analytical result under the applied voltage of over 1.3 kV.

Keywords: Self-excitation, Electrostatic actuator, Energy recovery, Elastic element

1. Introduction

Actuation and its related systems are some of the most important key technologies in industrial, rescue, medical, and many other fields. Actuators require various characteristics depending on their diversified applications[1]. These are also acceptable for miniaturized robots and micro mechatronic devices, which are widely studied and developed these days[2]. High energy density and simple structures are urgently required for these usages; hence, appropriate actuators are studied and developed to satisfy the following requirements: shape memory alloy[3, 4, 5, 6], piezo electric elements[7, 8, 9, 10], magnetostrictive elements[11, 12, 13, 14], and high polymer gel[15, 16, 17, 18], among others. Most of these are operated by controlling the voltage (or current) applied to the actuators, which has challenges in some cases like wireless operation, drive in high magnetic field etc.

Actuators using the self-excitation phenomenon represent one of the potential solutions for miniaturized devices because the driving equipment can be miniaturized not to employ converters or other elements. Self-excited actuation brings higher robustness and efficiency to oscillatory motions, especially for micro robots and mechatronic devices[19]. Self-excited electrostatic actuators, which are also known as Franklin bell or Gordon bell, are one of the simplest self-excited oscillators. The actuators oscillate with the DC voltage and the simple structures that are mainly composed of only two electrodes and a conductive armature.

The electrostatic force has high applicability to micro mechatronic devices, as can be seen from the fact that electrostatic actuators are mainly used in under submillimeter scales such as micro electro mechanical systems (MEMS)[20]. This is because the electrostatic force has a higher force density in a smaller scale with consideration of the scale effect.

These features of self-excited electrostatic actuators seem suitable for micro mechatronic devices, including miniaturized robots. Akio et al. developed an impact drive mechanism for one-way precise motion using the electrostatic self-excitation[21]. Inagaki et al. applied these actuators to a few types of robots and succeeded in drive of a walking robot and in the flapping motion of a flying robot[22]. Shmulevich et al. developed a self-excited electrostatic actuator thru a MEMS process [23]. Some studies were conducted as mentioned earlier, but these actuators only have small number of applications even in the research phase. Some challenges must be solved for more use of the self-excited electrostatic actuators. The high voltage required for actuation, damage by electrical discharge, and mechanical loss owing to collisions between the armature and electrodes are the main challenges keeping them from practical usage of self-excited electrostatic actuators. **Regarding high voltage, application of smaller size is also convenient for actuators using electrostatic force as well as in the view of the**

Email addresses: nabae@mes.titech.ac.jp (Hiroyuki Nabae), ikeda.k.au@m.titech.ac.jp (Koichi Ikeda)

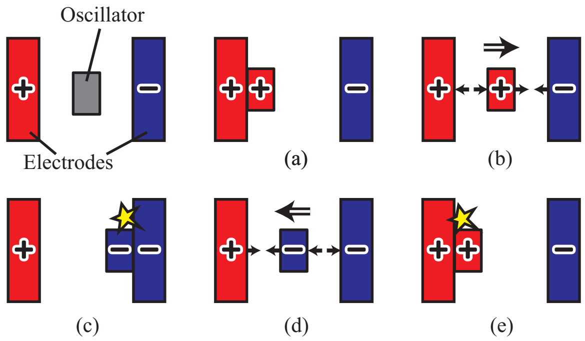

Figure 1: **General principle of the self-excited electrostatic actuator. (a) The armature has the same charge as the electrode (positive charge in the figure) by contacting one of the electrodes. (b) A repulsive force and an attractive force are generated between the armature and the positive and negative electrodes, respectively; hence, the armature moves to the negative electrode. (c) The armature contacts the negative electrode and has negative charge. (d) A repulsive force and an attractive force are generated between the armature and the negative and positive electrodes, respectively; hence, the armature moves to the positive electrode. (e) The armature contacts the positive electrode and has positive charge (return to (a)).**

scale effect because the same electric field can be generated by lower applied voltage.

This research focuses on the mechanical loss with collisions between the armature and electrodes and proposes a method for decreasing this loss by combining a self-excited electrostatic actuator and elastic elements. This study first conducts a model-based analysis for investigating the effect of the proposed method that combines electrostatic self-excitation and pure elastic elements. The damping effect is then considered through a simulation-based analysis. Moreover, the limitation of the proposed method is shown. After the analysis, the results are compared with those of an experiment conducted using a prototype device to evaluate the proposed method.

2. Concept of proposed method

Fig. 1 shows the general principle of the self-excited electrostatic actuator. The actuator mainly consisted of two electrodes and a conductive armature.

- **(a)** By contacting one of the electrodes, the armature is found to have the same charge as the electrode (positive charge in the figure).
- **(b)** A repulsive force and an attractive force are generated between the armature and the positive and negative electrodes, respectively; hence, the armature moves to the negative electrode.
- **(c)** The armature contacts the negative electrode and charges negative.
- **(d)** A repulsive force and an attractive force are generated between the armature and the negative and positive electrodes, respectively; hence, the armature moves to the positive electrode.

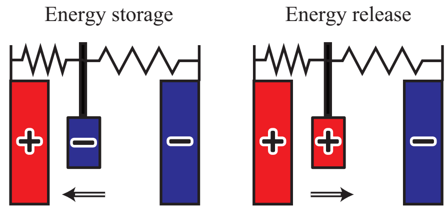

Figure 2: Concept of the proposed actuator that combines the self-excited electrostatic actuator and the elastic elements.

- **(e)** The armature contacts the positive electrode and charges positive (return to (a)).

The armature had collisions with the electrodes in (c) and (e) of Fig. 1. The collision is one of the main causes for the energy loss of the self-excited electrostatic actuators[24]. We proposed the addition of elastic elements to the actuator (Fig. 2) to decrease the energy loss. The kinematic energy was stored in the elastic elements as elastic energy when the armature moved to one of the electrodes. By storing the energy in the elastic elements, the loss energy by the collision was decreased because the velocity became small. The stored energy was recovered to the armature as kinematic energy when the armature moved away from the electrode. Most studies on self-excited electrostatic actuators support the armature by low resistant material or mechanisms like strings. This might come from the image that the electrostatic force is so low in a macro scale. The oscillator developed by Shmulevich et al. [23] supported the armature by elastic hinges. However, they did not mention about the effect of the elastic hinges. Furthermore, no analysis on the relationship between the oscillation characteristic and an elastic coefficient was conducted. The proposed method would not be only useful for practical usages of self-excited electrostatic actuators, but also purely interesting as a unique physical system.

3. Model-based analysis of the self-excited electrostatic actuator with the elastic element

This section analytically discusses the effect of an elastic element on electrostatic self-excitation. In the first step, a simple dynamic model of the proposed system was constructed considering a pure elastic effect. The effect of a damping factor was then discussed by a simulation.

Effect of the elastic element on the electrostatic self-excitation

Fig. 3 shows an analytical model with elastic elements. The armature was a conductive plate supported by an elastic element. **In this model, the thickness of the armature and hinge are assumed to be small enough to be ignored.** The DC voltage of V_c was applied between two electrodes. When the armature contacted one of the electrodes, the armature was charged with the same charge as the contacted electrode and experienced a repulsive force from the electrode and an attractive force from the other electrode. The armature then finally contacted the electrode of the opposite side, and the armature

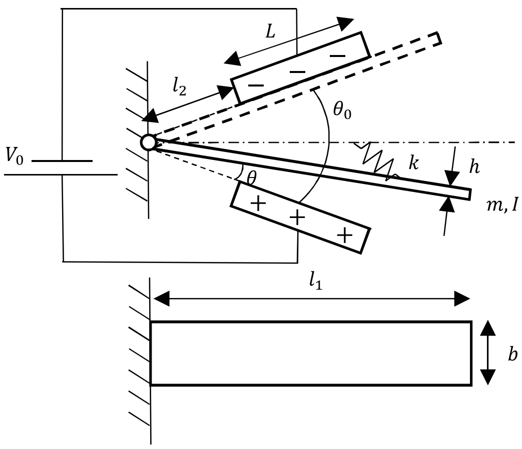

Figure 3: —**Analytical model for self-excited electrostatic actuator with pure elasticity. k means the elastic coefficient for the rotating motion of the armature.**

charged the same charge as the electrode. The DC voltage can generate an oscillating motion by repeating this process.

Various types of modeling approaches have been proposed for self-excited electrostatic actuators[21, 23, 25, 26]. This study employed a method based on the capacitance between the plates of the armature and electrodes, which were used in previous studies using plate-shaped armatures[21, 23]. Note that this study modeled a rotational case because of the easy preparation for an experimental evaluation. However, the system was essentially the same as a linear type with parallelly arranged electrodes. It also brought the same conclusion.

First, the capacitances between the electrodes and the armature of the minute area at a distance l from the center of rotation were calculated. The capacitances in the minute area $\mathrm{d}C_1$ and $\mathrm{d}C_2$ were in positive and negative sides, respectively. These values were obtained using a minute length $\mathrm{d}l$ as below:

$$\begin{cases} \mathrm{d}C_1(l) = \dfrac{\varepsilon_0 b}{l\theta}\mathrm{d}l, \\ \mathrm{d}C_2(l) = \dfrac{\varepsilon_0 b}{l(\theta_0 - \theta)}\mathrm{d}l. \end{cases} \tag{1}$$

When the rotating angle of the armature θ changes as $0 \rightarrow \theta_0$, $\theta_0 \rightarrow 0$, the armature has the charge $dQ_{0\rightarrow\theta_0}, dQ_{\theta_0\rightarrow 0}$:

$$\begin{cases} \mathrm{d}Q_{0\rightarrow\theta_0} = \dfrac{\varepsilon_0 b V_0}{l\theta_0}\mathrm{d}l \;\; (\theta : 0 \rightarrow \theta_0), \\ \mathrm{d}Q_{\theta_0\rightarrow 0} = -\dfrac{\varepsilon_0 b V_0}{l\theta_0}\mathrm{d}l \;\; (\theta : \theta_0 \rightarrow 0). \end{cases} \tag{2}$$

The charge $\mathrm{d}Q_{0\rightarrow\theta_0}$ and $\mathrm{d}Q_{\theta_0\rightarrow 0}$ were constant during θ: $0 \rightarrow \theta_0$ or $\theta_0 \rightarrow 0$, respectively; hence, $\mathrm{d}Q$ can be expressed as follows using $\mathrm{d}C_1$ and $\mathrm{d}C_2$:

$$\mathrm{d}Q = -(V_0 - V)\mathrm{d}C_1(l) + V\mathrm{d}C_2(l). \tag{3}$$

By substituting Eq. 1 to Eq. 3, the voltage between the armature and the ground V can be calculated as:

$$V = \begin{cases} \dfrac{\theta_0^2 - \theta^2}{\theta_0^2}V_0 & (\theta : 0 \rightarrow \theta_0), \\ \dfrac{(\theta_0 - \theta)^2}{\theta_0^2}V_0 & (\theta : \theta_0 \rightarrow 0). \end{cases} \tag{4}$$

If the equation of the parallel capacitance is substituted instead of Eq. 1, a parallel type model can be calculated. From Eqs. 3 and 4, the force $\mathrm{d}F$ working on the minute area of the armature was obtained by the equations below:

$$\mathrm{d}F = \begin{cases} \dfrac{\varepsilon_0 b V_0^2}{l^2\theta_0^2}\left(\dfrac{2\theta}{\theta_0} + 1\right)\mathrm{d}l & (\theta : 0 \rightarrow \theta_0), \\ \dfrac{\varepsilon_0 b V_0^2}{l^2\theta_0^2}\left(\dfrac{2\theta}{\theta_0} - 3\right)\mathrm{d}l & (\theta : \theta_0 \rightarrow 0). \end{cases} \tag{5}$$

The rotation moment by $\mathrm{d}F$ was calculated from Eq. 5 as:

$$\begin{aligned} \mathrm{d}M &= l\mathrm{d}F, \\ &= \begin{cases} \dfrac{\varepsilon_0 b V_0^2}{l\theta_0^2}\left(\dfrac{2\theta}{\theta_0} + 1\right)\mathrm{d}l & (\theta : 0 \rightarrow \theta_0), \\ \dfrac{\varepsilon_0 b V_0^2}{l\theta_0^2}\left(\dfrac{2\theta}{\theta_0} - 3\right)\mathrm{d}l & (\theta : \theta_0 \rightarrow 0). \end{cases} \end{aligned} \tag{6}$$

Integrating $\mathrm{d}M$ from l_2 to $l_2 + L$, the rotation moment acting on the armature was obtained as:

$$M = \begin{cases} \dfrac{\varepsilon_0 b V_0^2}{\theta_0^2}\log\left(1 + \dfrac{L}{l_2}\right)\left(\dfrac{2\theta}{\theta_0} + 1\right) & (\theta : 0 \rightarrow \theta_0), \\ \dfrac{\varepsilon_0 b V_0^2}{\theta_0^2}\log\left(1 + \dfrac{L}{l_2}\right)\left(\dfrac{2\theta}{\theta_0} - 3\right) & (\theta : \theta_0 \rightarrow 0). \end{cases} \tag{7}$$

An equation of motion in this system can be expressed as follows by adding the rotation moment of the elastic element $k(\theta - \theta_0/2)$ to Eq. 7:

$$I\ddot{\theta} = \begin{cases} \left\{\dfrac{2\varepsilon_0 b V_0^2}{\theta_0^3}\log\left(1 + \dfrac{L}{l_2}\right) - k\right\}\theta + \left\{\dfrac{\varepsilon_0 b V_0^2}{\theta_0^2}\log\left(1 + \dfrac{L}{l_2}\right) + \dfrac{k\theta_0}{2}\right\} \\ \hfill (\theta : 0 \rightarrow \theta_0), \\ \left\{\dfrac{2\varepsilon_0 b V_0^2}{\theta_0^3}\log\left(1 + \dfrac{L}{l_2}\right) - k\right\}\theta + \left\{-\dfrac{3\varepsilon_0 b V_0^2}{\theta_0^2}\log\left(1 + \dfrac{L}{l_2}\right) - \dfrac{k\theta_0}{2}\right\} \\ \hfill (\theta : \theta_0 \rightarrow 0). \end{cases} \tag{8}$$

where I is the moment of inertia of the armature and k means the elastic coefficient for the rotating motion of the armature.

The effect of elasticity was then discussed by considering the oscillating frequency f based on the obtained equation of motion Eq. 8. The variables A and B are defined as follows when the moment of inertia of the armature is expressed as $I = ml_1^2/3$:

$$\begin{cases} A = \dfrac{3}{ml_1^2}\left\{\dfrac{2\varepsilon_0 b V_0^2}{\theta_0^3}\log\left(1 + \dfrac{L}{l_2}\right) - k\right\}, \\ B = \dfrac{3}{ml_1^2}\left\{\dfrac{\varepsilon_0 b V_0^2}{\theta_0^2}\log\left(1 + \dfrac{L}{l_2}\right) + \dfrac{k\theta_0}{2}\right\}. \end{cases} \tag{9}$$

Eq. 8 can be simplified to the following using Eq. 9:

$$\ddot{\theta} = A\theta + B. \tag{10}$$

θ and $\dot{\theta}$ can be calculated as follows by focusing on the motion during $\theta : 0 \to \theta_0$ with initial velocity v_0:

$$\theta = \begin{cases} \frac{B + v_0\sqrt{A}}{2A}\exp\left(\sqrt{A}t\right) + \frac{B - v_0\sqrt{A}}{2A}\exp\left(-\sqrt{A}t\right) - \frac{B}{A} & (A > 0), \\ \frac{B}{2}t^2 + v_0 t & (A = 0), \\ \frac{B}{A}\cos\left(\sqrt{-A}t\right) - \frac{v_0\sqrt{-A}}{A}\sin\left(\sqrt{-A}t\right) - \frac{B}{A} & (A < 0). \end{cases} \tag{11}$$

$$\dot{\theta} = \begin{cases} \frac{B\sqrt{A} + v_0 A}{2A}\exp\left(\sqrt{A}t\right) - \frac{B\sqrt{A} - v_0 A}{2A}\exp\left(-\sqrt{A}t\right) & (A > 0), \\ Bt + v_0 & (A = 0), \\ \frac{B}{\sqrt{-A}}\sin\left(\sqrt{-A}t\right) + v_0\cos\left(\sqrt{-A}t\right) & (A < 0). \end{cases} \tag{12}$$

The elapsed time t_1 for travelling from $\theta = 0$ to θ_0 is obtained as follows from those equations:

$$t_1 = \begin{cases} \dfrac{\log\left(\dfrac{B + A\theta_0 + \sqrt{2AB\theta_0 + A^2\theta_0^2 + Av_0^2}}{B + v_0\sqrt{A}}\right)}{\sqrt{A}} & (A > 0), \\ \dfrac{-v_0 + \sqrt{2B\theta_0 + v_0^2}}{B} & (A = 0), \\ \dfrac{\cos^{-1}\left(\dfrac{-B^2 - AB\theta_0 - \sqrt{2A^2B\theta_0 v_0^2 + A^3\theta_0^2 v_0^2 + A^2 v_0^4}}{-B^2 + Av_0^2}\right)}{\sqrt{-A}} & (A < 0). \end{cases} \tag{13}$$

The velocity at contacting ($\theta = \theta_0$) v_1 is indicated as:

$$v_1 = \sqrt{2B\theta_0 + A\theta_0^2 + v_0^2}. \tag{14}$$

v_0 in the steady state is presented as follows because of $v_0 = ev_1$ in the steady state:

$$v_0 = e\sqrt{\frac{2B\theta_0 + A\theta_0^2}{1 - e^2}}. \tag{15}$$

Substituting Eq. 15 to Eq. 13, the oscillating frequency is obtained from the relationship $f = 1/t_1$.

$$f = \begin{cases} \dfrac{\sqrt{A}}{2\log\dfrac{(B + A\theta_0)\sqrt{1 - e^2} + \sqrt{A\theta_0(2B + A\theta_0)}}{e\sqrt{A\theta_0(2B + A\theta_0)} + B\sqrt{1 - e^2}}} & (A > 0), \\ \dfrac{B}{2\sqrt{2}(1 - e)\sqrt{\dfrac{B\theta_0}{1 - e^2}}} & (A = 0), \\ \dfrac{\sqrt{-A}}{2\cos^{-1}\dfrac{(B^2 + AB\theta_0)(1 - e^2) - A\theta_0(2B + A\theta_0)e}{B^2 - (B + A\theta_0)^2 e^2}} & (A < 0). \end{cases} \tag{16}$$

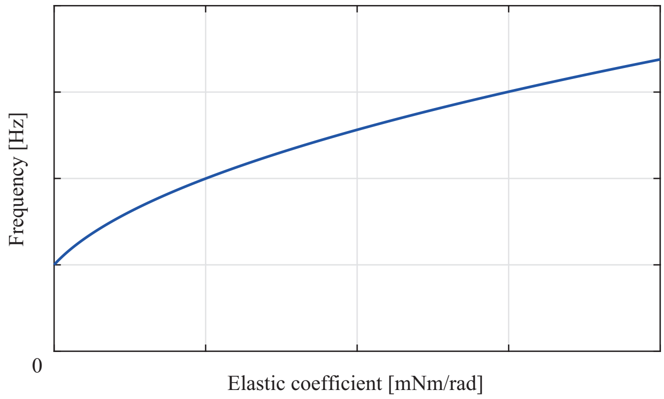

Figure 4: Typical relationship between the elasticity and the oscillating frequency of the self-excited electrostatic actuator with pure elasticity. The oscillating frequency increases as the elastic coefficient becomes larger.

The oscillating frequency f can be obtained as a function of k by substituting A, B to Eq. 16. Fig. 4 shows the typical relationship between the elasticity and the oscillating frequency obtained from Eq. 16. The oscillating frequency increased according to the increase of k in Fig. 4. However, the actuator was not able to continue oscillating under a large elasticity k because of the losses caused by the air resistance, mechanical damping, etc. The effect of the damping factor was discussed herein based on the simulation in this section.

3.1. Damping factor effect

This subsection discussed the effect of the damping factor on the self-excited electrostatic actuator with an elastic element. The equation of motion is expressed as follows by adding the damping factor to Eq. 8, which is written as $c\dot{\theta}$ using damping coefficient c and angular velocity $\dot{\theta}$. This study uses a damping factor, whose resistance is proportional to the squared value of the velocity because of the estimation that the oscillating motion is fast enough.

$$I\ddot{\theta} = \begin{cases} (A - k)\theta - c\dot{\theta}\left|\dot{\theta}\right| - \frac{(k - A)\theta_0}{2} + A\theta_0 & (\theta : 0 \to \theta_0), \\ (A - k)\theta - c\dot{\theta}\left|\dot{\theta}\right| - \frac{(k - A)\theta_0}{2} - A\theta_0 & (\theta : \theta_0 \to 0). \end{cases} \tag{17}$$

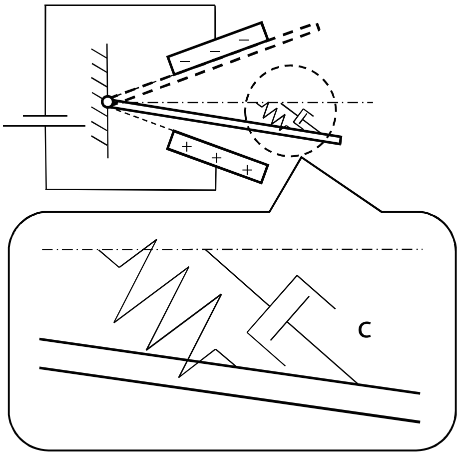

Figure 5: Spring and damper model for the analysis.

where

$$A = \frac{2\varepsilon_0 b V_0^2}{\theta_0^3}\log\left(1+\frac{L}{l_2}\right). \quad (18)$$

The model is expressed by Eq. 17 and the restitution condition in the collision of the armature with the electrodes. As an analytical approach has difficulty owing to discontinuity in the collisions, a numerical approach is conducted in this paper. A numerical simulator that calculates the motion of the prototype actuator was programmed based on Eq. 3 by using Simulink (MathWorks). In an actual operation, this simulation is conducted using a fourth-order Runge–Kutta method, which is most commonly used because of its appropriate accuracy and simplicity, using commercial software (Simulink, MathWorks, Inc.). Table 1 lists the main parameters for the simulations. The damping coefficient for the simulation was experimentally determined by averaging the experimental values obtained from the displacement waveform of the armature of each width in the free oscillation using the prototype device with no applied voltage. The elastic coefficient values were also obtained by the displacement profile of the free oscillation. Table 2 lists the natural frequency f_n [Hz], elastic coefficient k [Nm/rad], and damping coefficient c [Nm(rad/s)$^{-2}$]of the armature in each hinge width of a.

The damping coefficients were almost constant in Table 2. This tendency indicated that the air resistance of the armature was dominant compared to the internal damping of the CFRP hinges.

Fig.6 shows the relationship between the elasticity and the oscillating frequency with the damping factor. The damping factor set to be constant (c=7.2 × 10^{-7} [Nm(rad/s)$^{-2}$]) because of the assumption that the main damping factor comes from the air resistance of the armature. The increase of the oscillating frequency can also be observed when the elasticity becomes larger, as seen in the analysis without the damping factor. However, the result differed in that the self-excited oscillation did not occur with very large elastic coefficients. The critical point was expressed by a cross mark. Considering an oscillation period, the energy loss caused by the damping factor increased according to the larger velocity (frequency), while the work done by the electrostatic force on the armature was the same. Note that the work done by the elastic element on the armature is ideally zero. The energy loss of the armature exceeded the work by the electrostatic force at the steady-state frequency over some values of the elastic coefficient. In addition, the oscillating frequency slightly decreased just before the point, where the self-excited oscillation stopped. In this manner, the elastic coefficient should be appropriately selected according to the damping characteristics of a system subjected to be applied.

Table 1: Parameters for simulation and experiment.

Parameter	Symbol	Value
Width of the hinge	a	2.0, 4.0, 6.0, 8.0, 10.0 ×10^{-3} [m]
Width of the armature	b	10.0×10^{-3} [m]
Angle between the electrodes	θ_0	3.6×10^{-2} [rad]
Mass of inertia	m	8.4×10^{-5} [kg]
Permittivity of vacuum	ε_0	8.85×10^{-12} [F/m]
Coefficient of restitution	e	0.0 [-]
Moment of inertia	I	2.5×10^{-8}[Kgm^2]
Applied voltage	V_0	0.9, 1.0, 1.1, 1.2, 1.3, 1.4, 1.5 ×10^3 [V]
Length of the armature	l_1	30.0×10^3 [m]
Distance between the electrode and the rotation center	l_2	15.0×10^{-3} [m]
Length of the hinge	l_3	1.5×10^{-3} [m]
Thickness of the armature	h	0.2×10^{-3} [m]
Length of the electrode	L	10.0×10^{-3} [m]

Table 2: Natural frequency f_n [Hz], elastic coefficient k [Nm/rad], and damping coefficient c [Nm(rad/s)$^{-2}$] of the armature in each hinge width of a.

a [m]	f_n [Hz]	k [Nm/rad]	c [Nm(rad/s)$^{-2}$]
2.0×10^{-3}	70.5	4.9×10^{-1}	8.8×10^{-7}
4.0×10^{-3}	97.0	9.4×10^{-1}	7.9×10^{-7}
6.0×10^{-3}	109.6	1.2×10^{-2}	4.4×10^{-7}
8.0×10^{-3}	116.8	1.4×10^{-2}	6.3×10^{-7}
10.0×10^{-3}	124.3	1.5×10^{-2}	8.9×10^{-7}

4. Experimental evaluation and discussions

This section confirmed the results of the previous section by an experiment. A prototype oscillator was designed to test the oscillation characteristic with various values of the elastic coefficient.

4.1. Experimental setup

Fig. 7 shows a schematic figure of a prototype oscillator used to evaluate the proposed method. Fig. 8 also presents a photo

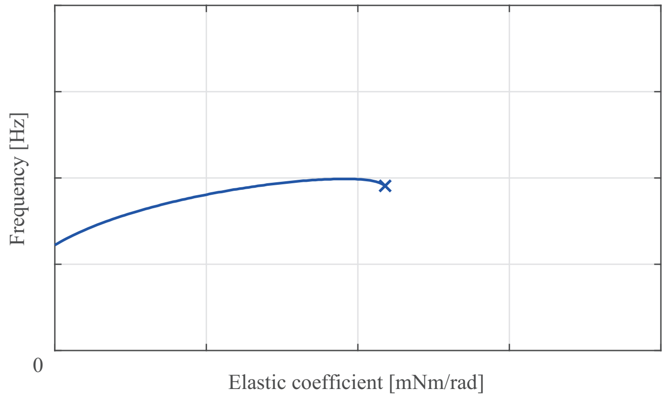

Figure 6: Typical relationship between the elasticity and the oscillating frequency of the self-excited electrostatic actuator with elasticity considering the damping factor. The oscillating frequency increases as the elastic coefficient becomes larger. The oscillation stops in a critical value. The point of the critical value is indicated by a cross mark.

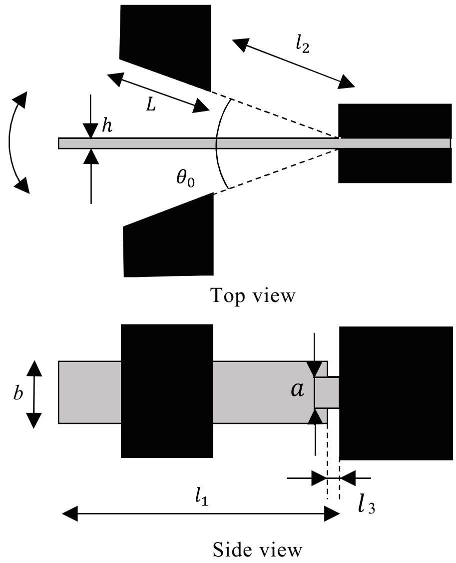

Figure 7: Schematic figure of the prototype for measurement. The elastic coefficient can be controlled by changing the width of the hinge a.

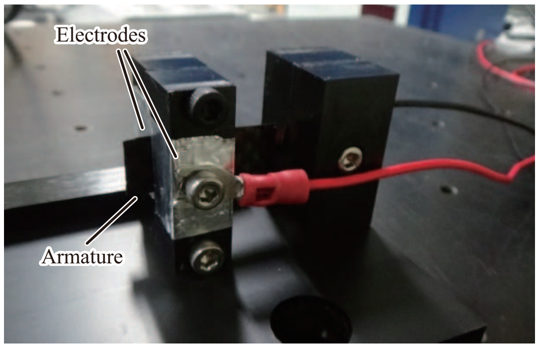

Figure 8: Photo of the prototype device.

of the prototype device. The prototype oscillator was mainly composed of an armature made of carbon fiber-reinforced plastic (CFRP), electrodes made of thin aluminum membrane, and a body made of polyacetal. Elasticity was installed as a bending modulus of a 0.2 mm-thick CFRP plate and controlled by changing the hinge width a in Fig. 7. Fig. 9 shows a simple measurement system prepared for the basic evaluation of the prototype oscillator motion. The input voltage was applied to the oscillator by a high-voltage amplifier (MODEL 2210, Trek). The displacement of the oscillator was obtained by a laser displacement sensor (LK-G32, LK-G3000V, Keyence Corporation). The current value was obtained using a current probe (TCPA300, Tectronix). The data of the voltage, current, and displacement were recorded and processed by a digital signal processor (DS1104, DSpace).

4.2. Evaluation results and discussions

This subsection described the experimental evaluation using the experimental setup mentioned earlier. In the experiment, the oscillator was applied with a voltage from 900 V to 1500 V by 100 V steps each. The elastic coefficients were 0.49, 0.94, 1.2, 1.4, and 1.5 $\times 10^{-2}$ Nm/rad, which corresponded to a = 2.0, 4.0, 6.0, 8.0, and 10.0 $\times 10^{-3}$ [m], respectively. The displacement was measured by five times at each voltage and elastic coefficient. Fig. 10 represents the typical displacement profile results of the simulation (Fig. 10(a)) and the experiment (Fig. 10(b)). The operating voltage was 1300 V, and the elastic coefficient was 1.2 $\times 10^{-2}$ Nm/rad. The displacement profile in the experimental results exhibited a particular waveform, which was like a triangle wave, but consisted of curve lines. The featured profile was successfully expressed by the simulation, which may be caused by the acceleration and the sudden change of the driving direction at the electrodes. The oscillation frequency was calculated from the abovementioned displacement data. The experimental results were then compared with the simulation results. The experimental frequency was obtained by the mean values of the experimental values by five times. The standard deviation was also calculated. The value of the fifth to tenth period of oscillation was used to identify the simulation value of the frequency. Fig. 11 shows the results of the comparison of the experimental and simulation frequencies. The simulation and experimental values were expressed by solid lines and open symbol plots, respectively. The critical values obtained by the simulation were expressed by the cross marks at the end of the lines. First, the increase of the oscillating frequency was successfully observed in the experiment. The simulation predicted the oscillation frequency and the limiting elastic coefficients indicated as cross marks.

Regarding the frequency values, the results had large differences between the simulation and the experiment under low voltages and elastic coefficients. The difference decreased according to the increase of the voltage and the elastic coefficient. The error values with the elastic coefficient of 0.49×10^{-2} [Nm/rad] under 0.9, 1.0, 1.1, and 1.2 kV were 35.6, 26.0, 20.0, and 16.8%, respectively. The error values with the

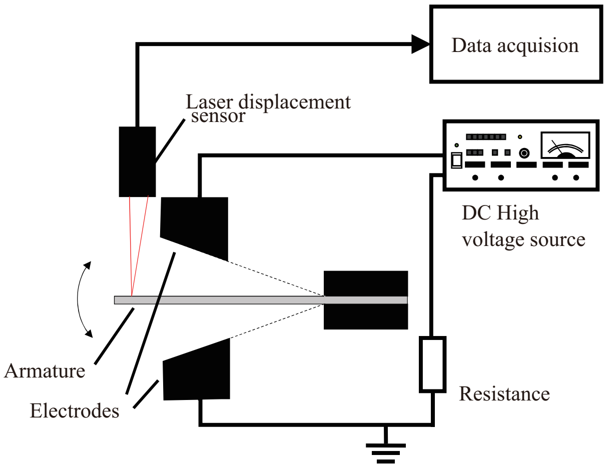

Figure 9: System configuration for the experiments of the displacement measurement.

elastic coefficients of 0.49, 0.94 [Nm/rad] under 0.9 kV were 35.6, 4.1%, respectively. Meanwhile, the errors became small under high voltages. The average value of the error was 6.4% over 1.3 kV. These errors would be caused by the dimensional errors of the prototype. Therefore, the error became small as the thrust force (torque) was increased by the high applied voltage and the large elastic coefficient.

The critical value shifted to the higher side of the elastic coefficients with a larger applied voltage in the simulation. The work on the armature by the electrostatic force was increased by the larger charges on the electrodes and the armature caused by the higher applied voltage. Accordingly, it can consume the energy by the air resistance in the oscillatory motion with a higher frequency. This tendency can be observed in the experimental results. The actuator can drive only with k = 0.49 and 0.94 $\times 10^{-2}$ [Nm/rad] when the applied voltage was 0.9 kV. Meanwhile, the actuator oscillated with $k = 1.2 \times 10^{-2}$ [Nm/rad] when the voltage was set to be 1.0, 1.1, and 1.2 kV. When increasing the applied voltage further (1.3, 1.4, and 1.5 kV), the actuator generated self-excitation with higher elastic coefficients (k = 1.4, 1.5 $\times 10^{-2}$ [Nm/rad]). Although the experimental and simulation results showed the same tendency as mentioned earlier, some differences were observed between the simulation and the experiment. When the voltage values were 1.0, 1.1, and 1.2 kV, the self-excited oscillation did not occur with k=1.4, 1.5 $\times 10^{-2}$ [Nm/rad] in spite of far smaller elastic coefficients than the critical values obtained by the simulation. This difference may come from the complicated air flow generated by the oscillating motion of the plate in the small gap. In other words, the air flow affected the physical system of the oscillator to drop the critical values of the elastic coefficient. **The fringing effect[27, 28] of the electric field also could be one of the reasons for the errors in the frequencies and critical values.**

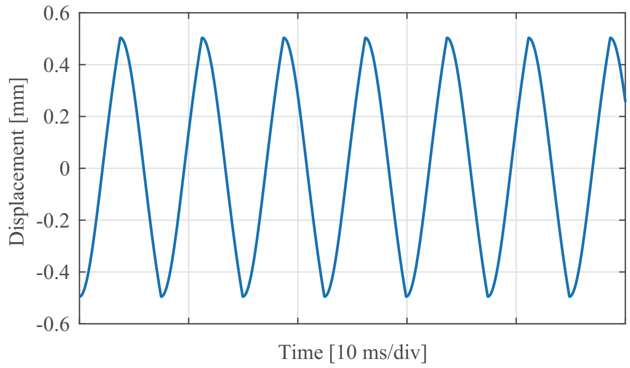

(a) Simulation

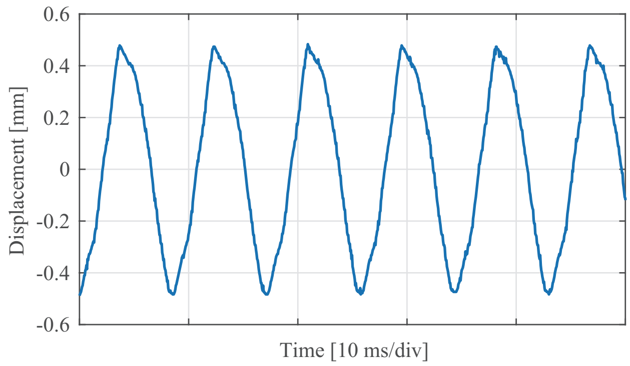

(b) Experiment

Figure 10: Typical response of the displacement during the oscillation. The operating voltage is 1300 V, and the elastic coefficient is 1.2 $\times 10^{-2}$ Nm/rad.

5. Conclusions

This study focused on the self-excited electrostatic actuators, which are one of the simplest oscillators among various types of actuators. The actuators oscillated with the DC voltage and the simple structures mainly composed of only two electrodes and a conductive armature. These features seemed suitable for micro mechatronic devices, including micro robots. However, some challenges remained, keeping the high voltage for actuation, damage by electrical discharge, and mechanical loss with collisions between the armature and the electrodes away from practical usages. This research focused on the mechanical loss with collisions between the armature and the electrodes and proposed a method for decreasing this loss by energy restoring with elastic elements. This study first conducted a model-based analysis of the behavior of the proposed system that combined electrostatic self-excitation and elastic elements. The analysis predicted that the oscillating frequency of the actuator becomes higher by increasing the elastic coefficient. The effect of the damping factor was then numerically analyzed. The simulation with the damping factor revealed the critical value, where the actuator stopped the self-excitation according to the increase of the elastic coefficient. This phenomenon was considered to come from the excess of loss energy by the damping factor over the work by the electrostatic force. The following point was considered to verify the simulation results: increase of the os-

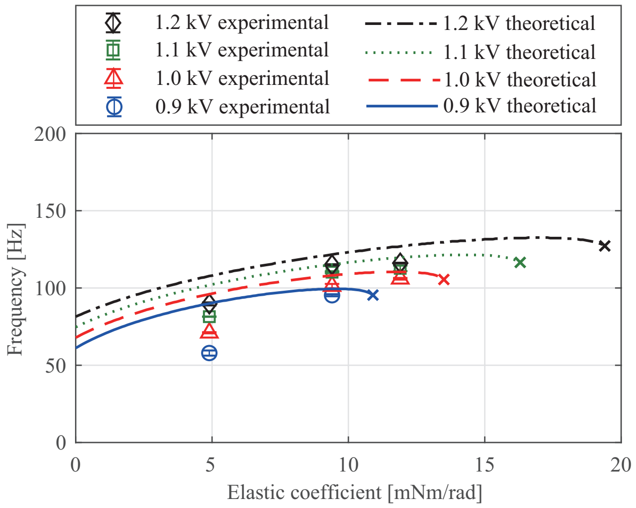

(a) 1000 V to 1200 V

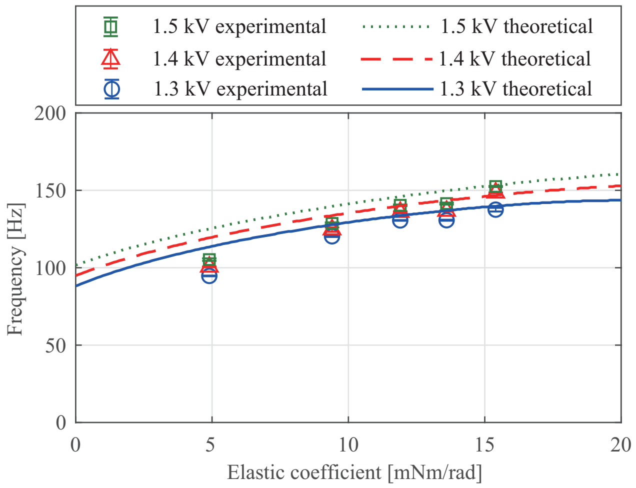

(b) 1300 V to 1500 V

Figure 11: Comparison of the frequencies between the experimental and simulation results. Both results of the relationship between the elastic coefficient and the oscillating frequency show positive correlations.

cillation frequency by elasticity and the critical value existence. We prepared a prototype of a self-excited electrostatic actuator that can change the value of the elastic coefficient. The experimental results successfully showed the same tendency as the aforementioned prediction obtained by the numerical analysis. From a quantitative point of view, the experimentally obtained frequency values had large errors under low voltage and elastic coefficients. These errors are caused by the low force or torque compared to any disturbance. At over 1.3 kV of the applied voltage, the results of the experimental verification matched the analytical results, and the experimentally obtained frequencies had errors less than 6.4% compared with the analytical result. The results succeeded in demonstrating the efficiency of the proposed method. **Meanwhile, there are some open challenges for actual applications: discharge between the armature and electrodes, driving characteristic with complex outer loads, etc.** We believe that this proposal could be the foundation for further development of micro mechatronic devices and miniaturized locomotive robots in the future.

References

[1] M. Zupan, M. F. Ashby, N. A. Fleck, Actuator classification and selection?the development of a database, Advanced Engineering Materials 4 (12) (2002) 933–940.

[2] S. A. Wilson, R. P. Jourdain, Q. Zhang, R. A. Dorey, C. R. Bowen, M. Willander, Q. U. Wahab, S. M. Al-hilli, O. Nur, E. Quandt, et al., New materials for micro-scale sensors and actuators: An engineering review, Materials Science and Engineering: R: Reports 56 (1-6) (2007) 1–129.

[3] K. Ikuta, M. Tsukamoto, S. Hirose, Shape memory alloy servo actuator system with electric resistance feedback and application for active endoscope, in: Robotics and Automation, 1988. Proceedings., 1988 IEEE International Conference on, Ieee, 1988, pp. 427–430.

[4] S. Hattori, M. Hara, H. Nabae, D. Hwang, T. Higuchi, Design of an impact drive actuator using a shape memory alloy wire, Sensors and Actuators A: Physical 219 (2014) 47–57.

[5] J. M. Jani, M. Leary, A. Subic, M. A. Gibson, A review of shape memory alloy research, applications and opportunities, Materials & Design (1980-2015) 56 (2014) 1078–1113.

[6] H. Rodrigue, W. Wang, M.-W. Han, T. J. Kim, S.-H. Ahn, An overview of shape memory alloy-coupled actuators and robots, Soft robotics 4 (1) (2017) 3–15.

[7] T. Higuchi, Y. Yamagata, K. Furutani, K. Kudoh, Precise positioning mechanism utilizing rapid deformations of piezoelectric elements, in: Micro electro mechanical systems, 1990. Proceedings, an investigation of micro structures, sensors, actuators, machines and robots. IEEE, IEEE, 1990, pp. 222–226.

[8] H. Adriaens, W. L. De Koning, R. Banning, Modeling piezoelectric actuators, Mechatronics, IEEE/ASME Transactions on 5 (4) (2000) 331–341.

[9] I. Chopra, Review of state of art of smart structures and integrated systems, AIAA journal 40 (11) (2002) 2145–2187.

[10] M. Moory-Shirbani, H. M. Sedighi, H. M. Ouakad, F. Najar, Experimental and mathematical analysis of a piezoelectrically actuated multilayered imperfect microbeam subjected to applied electric potential, Composite Structures 184 (2018) 950–960.

[11] T. Ueno, E. Summers, M. Wun-Fogle, T. Higuchi, Micro-magnetostrictive vibrator using iron–gallium alloy, Sensors and Actuators A: Physical 148 (1) (2008) 280–284.

[12] Z. G. Zhang, T. Ueno, T. Higuchi, Magnetostrictive actuating device utilizing impact forces coupled with friction forces, in: Industrial Electronics (ISIE), 2010 IEEE International Symposium on, IEEE, 2010, pp. 464–469.

[13] J. Atulasimha, A. B. Flatau, A review of magnetostrictive iron–gallium alloys, Smart Materials and Structures 20 (4) (2011) 043001.

[14] H. García-Miquel, D. Barrera, R. Amat, G. Kurlyandskaya, S. Sales, Magnetic actuator based on giant magnetostrictive material terfenol-d with strain and temperature monitoring using fbg optical sensor, Measurement 80 (2016) 201–206.

[15] R. Kanno, S. Tadokoro, M. Hattori, T. Takamori, M. Costaftis, K. Oguro, Dynamic model of icpf (ionic conducting polymer film) actuator, in: Systems, Man and Cybernetics, 1995. Intelligent Systems for the 21st Century., IEEE International Conference on, Vol. 1, IEEE, 1995, pp. 177–182.

[16] K. Asaka, K. Oguro, Y. Nishimura, M. Mizuhata, H. Takenaka, Bending of polyelectrolyte membrane–platinum composites by electric stimuli i. response characteristics to various waveforms, Polymer Journal 27 (4) (1995) 436.

[17] M. Shahinpoor, Y. Bar-Cohen, J. Simpson, J. Smith, Ionic polymer-metal composites (ipmcs) as biomimetic sensors, actuators and artificial muscles-a review, Smart materials and structures 7 (6) (1998) R15.

[18] Q. Shen, S. Trabia, T. Stalbaum, V. Palmre, K. Kim, I.-K. Oh, A multiple-shape memory polymer-metal composite actuator capable of programmable control, creating complex 3d motion of bending, twisting, and oscillation, Scientific reports 6 (2016) 24462.

[19] K. Ono, T. Okada, Self-excited vibratory system for a flutter mechanism (special issue on nonlinear dynamics), JSME International Journal Series C Mechanical Systems, Machine Elements and Manufacturing 41 (3) (1998) 621–629.

[20] J. W. Judy, Microelectromechanical systems (mems): fabrication, design and applications, Smart materials and Structures 10 (6) (2001) 1115.
[21] A. Yamamoto, H. Katsurai, T. Higuchi, Dc-operated electrostatic impact drive actuator, Advanced Robotics 24 (10) (2010) 1441–1459.
[22] H. Inagaki, A. Saito, Flapping electrostatic actuator for micro-mobile=mechanisms, in: Proceedings of Poster and Video Exhibition, 1995, pp. 64–68.
[23] S. Shmulevich, I. Hotzen, D. Elata, The electromechanical response of a self-excited mems franklin oscillator, in: Micro Electro Mechanical Systems (MEMS), 2015 28th IEEE International Conference on, IEEE, 2015, pp. 41–44.
[24] M. Forjan, M. Marhl, V. Grubelnik, Mathematical modelling of the electrostatic pendulum in school and undergraduate education, European Journal of Physics 35 (1) (2013) 015022.
[25] D. Martin, R. Longbrake, An electrostatic oscillator experiment, American Journal of Physics 40 (1972) 395–398.
[26] K. Asano, On the theory of an electrostatic pendulum oscillator, American Journal of Physics 43 (1975) 423–427.
[27] H. B. Palmer, The capacitance of a parallel-plate capacitor by the schwartz-christoffel transformation, Electrical Engineering 56 (3) (1937) 363–368.
[28] R. S. Elliott, Electromagnetics: History, theory, and applications, IEEE press Piscataway, NJ, 1993.

Biographies

Hiroyuki Nabae received his B.E., M.E., and Ph.D. degrees from University of Tokyo, Tokyo, Japan in 2010, 2012, and 2015, respectively. He worked as a JSPS research fellow from April 2013 to March 2015. He is currently an assistant professor at Tokyo Institute of Technology. His research interests include mechatronics, robotics, and actuators.

Koichi Ikeda received his B.E. degree from Tokyo Institute of Technology, Japan in 2018. He is currently a master course student at Tokyo Institute of Technology. His research interests include actuators, robotics, and micro engineering.